ELSEVIER

Ductility of thin metal films on polymer substrates modulated by interfacial adhesion

Teng Li [1], Z. Suo [*]

Division of Engineering and Applied Sciences, Harvard University, Cambridge, MA 02138, USA

Abstract

When a laminate of a thin metal film on a tough polymer substrate is stretched, the metal film may rupture at strains ranging from a few percent to a few tens of percent. This variation in the ductility of the metal film is modulated by the adhesion of the metal/polymer interface. To study this modulation, here we use the finite element method to simulate the co-evolution of two processes: debonding along the interface and necking in the metal film. We model the interface as an array of nonlinear springs, and model the metal and the polymer as elastic–plastic solids. The simulation shows that necking of the film is accommodated mainly by interfacial sliding, rather than interfacial opening. Depending on the resistance of the interface to sliding, the metal film can exhibit three types of tensile behavior: the film slides and ruptures at a small strain by forming a single neck, the film slides and deforms to a large strain by forming multiple necks, and the film deforms uniformly to a very large strain without sliding and necking.
© 2006 Elsevier Ltd. All rights reserved.

Keywords: Metal film; Polymer substrate; Ductility; Adhesion; Necking; Sliding

1. Introduction

Flat-panel displays are rapidly replacing cathode-ray tubes as the monitors of choice for computers and televisions, a commercial success that has opened the era of macroelectronics, in which transistors and other micro-components are integrated over large areas. In addition to the flat-panel displays (Crawford, 2005), other macroelectronic products include X-ray imagers, thin-film solar cells, and thin-film antennas (Nathan and Chalamala, 2005). Like a micro-electronic product, a macroelectronic product consists of many thin-film components of small features. While micro-electronics advances by miniaturizing features, macroelectronics

---
[*] Corresponding author. Tel.: +1 617 4953789; fax: +1 617 4960601.
E-mail addresses: lit@umd.edu (T. Li), suo@deas.harvard.edu (Z. Suo).
[1] Present address: Department of Mechanical Engineering, University of Maryland, College Park, MD 20742, USA. Tel.: +1 301 4050364; fax: +1 301 3149477.

does so by enlarging systems. Macroelectronic products today are mostly fabricated on substrates of glass or silicon; they are expensive, fragile and not readily portable when their areas are large. To reduce cost and enhance portability, future innovation will come from new choice of materials and of manufacturing processes. For example, thin-film devices on thin polymer substrates lend themselves to roll-to-roll fabrication, resulting in lightweight, rugged and flexible products. These macroelectronic products will have diverse architectures, hybrid materials, and small features. Their mechanical behavior during manufacturing and use poses significant challenges (Suo et al., 2005).

This paper focuses on an issue specific to flexible macroelectronics: the tensile behavior of a thin metal film grown on a polymer substrate. These thin metal films are widely used as electrodes and interconnects. Recent experiments have suggested that the rupture strain of such a metal film is sensitive to its adhesion to the polymer substrate (Xiang et al., 2005). To study this effect, here we use the finite element method to simulate the co-evolution of two processes: debonding of the metal/polymer interface and necking of the metal film. We will show that the rupture strain of the metal film is modulated by interfacial sliding.

It has been often reported that thin metal films, freestanding or polymer-supported, rupture at small strains (<2%, Pashley, 1960; Chiu et al., 1994; Huang and Spaepen, 2000; Alaca et al., 2002; Gray et al., 2004; Xiang and Vlassak, 2005). On the other hand, it has also been reported that some polymer-supported metal films can sustain strains up to 20% (Kang, 1996; Macionczyk and Bruckner, 1999; Gruber et al., 2003). The cause for the substantial difference in rupture strain has been uncertain, but our recent work may have shed light on the subject.

Under tension, a freestanding thin metal film can deform plastically. When the tensile strain is large enough to break native oxides or other passivation layers on the surface of the metal film, dislocations in the metal film can readily exit. On further straining, the film does not harden as much as its bulk counterpart. Consequently, once the film thins preferentially at a local spot by forming a neck, further deformation is localized in the neck, leading to rupture (Fig. 1a). By volume conservation, local thinning results in a local elongation of length comparable to the film thickness. However, the local elongation contributes little to the overall rupture strain, because the film has an extremely small thickness-to-length ratio.

While the local elongation is accommodated for the freestanding metal film by the ruptured halves moving apart, it cannot be so accommodated for a metal film bonded to a substrate. This constraint of the substrate retards strain localization, so that the metal film can deform uniformly to a large strain (Fig. 1b). The above arguments are phrased in terms of necking, but similar arguments apply to localization by shear band formation. Indeed, for such a metal film on a polymer substrate, our recent finite element simulation and linear bifurcation analysis have shown that the substrate can retard strain localization and carry the film to a large strain (Li et al., 2005). For example, the simulation shows that a Cu film well adherent to a polyimide substrate should sustain strains in excess of 80%.

Our recent experiments with Cu films on polyimide substrates show that the rupture strains of the metal films are sensitive to their adhesion to the substrates (Xiang et al., 2005). Poorly bonded Cu films form channel
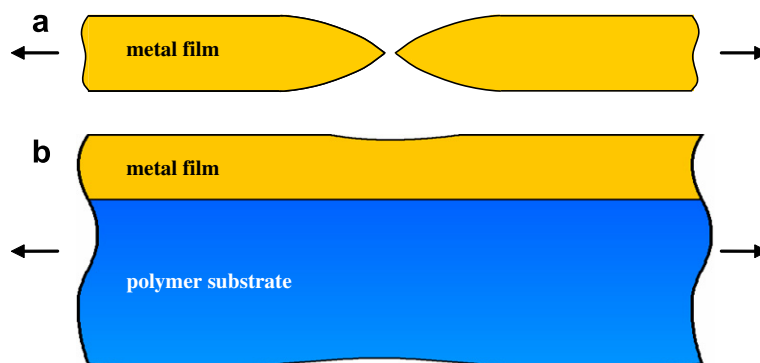

Fig. 1. The rupture of a metal film is caused by strain localization. Local thinning leads to local elongation. (a) A freestanding metal film accommodates the local elongation as the ruptured halves move apart. (b) When the film is well-bonded to a substrate, the local elongation in the film may be suppressed by the substrate.
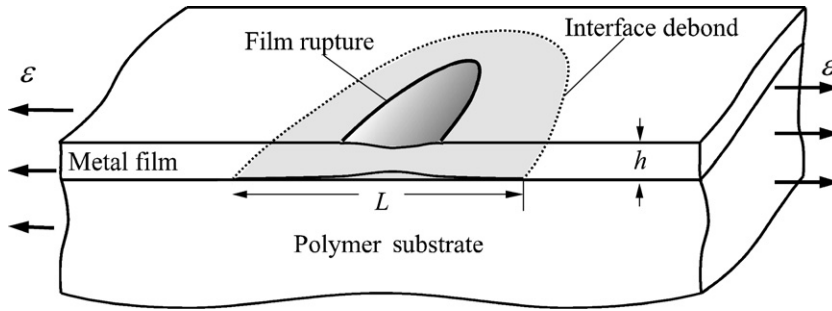
Fig. 2. A metal film is initially bonded to a thick polymer substrate. Subject to a tensile strain, the film necking and the interfacial debonding co-evolve. The rupture occurs by localized elongation in a segment of the film, of length comparable to the film thickness, but debond spreads over a segment of the interface many times the film thickness.

cracks at strains about 2%, while well-bonded Cu films can sustain strains up to 10% without appreciable cracks. At strains of 30%, however, all our Cu films do form zig-zag cracks.

The discrepancy in the rupture strain between the experiment and the theory may be caused by debonding between the films and the substrates. If the metal film debonds from the substrate, the film becomes freestanding and is free to form a neck. When the intact metal/polymer laminate is subject to a modest tensile strain, we expect strain localization and debonding to *co-evolve* (Fig. 2). Without debonding, the polymer substrate suppresses strain localization in the metal. Without localization, no traction is exerted on the interface to cause debonding. The conundrum parallels that of the co-evolution of debonding and buckling of a compressive film on a substrate (Hutchinson and Suo, 1992).

The effect of debonding on the rupture strain can be estimated as follows. The debonded portion of the film acts like a freestanding film under a tensile test. The debonding length, L, serves as the gauge length in the tensile test, so long as the polymer is sufficiently stiff. As the film approaches rupture, the local thinning gives a local elongation of magnitude proportional to the film thickness, h. The rest of the film is strained to the level approximately of the necking limit of a freestanding film, ε_N. Consequently, when the partially debonded film ruptures, the applied strain, estimated by the net elongation of the debonded film divided by the debonding length, is

$$\varepsilon \approx \varepsilon_N + \alpha h/L, \tag{1}$$

where α is a dimensionless number of order unity. The larger the debonding length, the smaller the rupture strain. To knock down the rupture strain to the order of a few percent, the debonding length has to be about 100 times the film thickness. The above estimate agrees with the results of finite element simulation on partially debonded metal films on polymer substrates (Li et al., 2005).

So far, the available experimental evidence and simulation results on the effect of adhesion on rupture strain are suggestive, but preliminary: the co-evolution of debonding and necking of the metal films has not been observed directly, and the quantitative relation between the adhesion parameters and the rupture strain remains uncertain. To address these concerns and plan further experiments, this paper studies the co-evolution of debonding and necking using the finite element method. Section 2 describes the computational model and discusses parameters of physical significance for the rupture process. Based on the simulation, Section 3 describes three types of tensile behavior, depending on both the interfacial strengths and the corresponding interfacial displacements. Section 4 further shows that necking in the film is mainly accommodated by interfacial sliding, not by interfacial opening. The effect of the interfacial shear strength on the rupture strain is then compared with that of the interfacial tensile strength.

2. Computational model

We use the finite element code ABAQUS v6.5 to simulate the co-evolution of debonding along the metal/polymer interface and necking in the metal film. In the finite element model, the film is a layer of thickness h,

and the substrate is a block of thickness $100h$ and length $80h$. The horizontal displacement is set to be zero along the centerline of the laminate, and set to be u along both sides of the laminate. The quantity $u/40h$ will be called the applied strain. The laminate is taken to deform under the plane strain conditions. Uniform deformation is a trivial solution to this boundary value problem. An imperfection is introduced to induce nonuniform deformation. At the center of the film surface, we place a V-shaped notch, $0.2h$ wide and $0.02h$ deep. Our previous simulations indicated that the geometric details of the notch affect quantitative predictions, but not qualitative behavior (Li et al., 2004). Taking advantage of symmetry we model only the right half of the laminate. Four-node quadrilateral plane strain elements are used for the film and the substrate. The film has 10 layers of elements in the thickness direction and a comparable element size in the length direction. The substrate is meshed with matched elements at the film/substrate interface, and coarser elements far away from the interface.

Both the metal and the polymer are modeled as elastic–plastic solids, obeying the J_2 deformation theory. Under uniaxial tension, the true stress σ and the natural strain ε follow the relation

$$\sigma = \begin{cases} \sigma = E\varepsilon, & \varepsilon \leqslant \sigma_Y/E, \\ \sigma_Y\left(\frac{\varepsilon}{\sigma_Y/E}\right)^N, & \varepsilon > \sigma_Y/E, \end{cases} \tag{2}$$

where E is Young's modulus, N the hardening exponent, and σ_Y the yield strength. In the simulations, the following values are used: $E = 100\,\text{GPa}$, $N = 0.02$, and $\sigma_Y = 100\,\text{MPa}$ for the metal; and $E = 8\,\text{GPa}$, $N = 0.5$ and $\sigma_Y = 50\,\text{MPa}$ for the polymer. These values are representative of a weakly hardening metal and a steeply hardening polymer (i.e., a polyimide).

As illustrated in Fig. 3, the metal/polymer interface is modeled as an array of nonlinear springs, characterized by a tensile and a shear traction–displacement law, with six parameters: interfacial tensile strength σ_n and shear strength σ_s, corresponding opening displacement δ_n and sliding displacement δ_s, and the areas under the traction–displacement curves Γ_n and Γ_s. The interface is meshed with four-node cohesive elements sharing nodes with the neighboring elements in the film and the substrate. In some cases of simulation, the debonded film and the substrate may slightly interpenetrate. The interpenetration could be avoided by using the contact element available in ABAQUS, but this option is not used in this study.

In describing the simulations, we will use two types of dimensionless groups: $\delta_{n,s}/h$ and $\sigma_{n,s}/\sigma_Y^m$, where σ_Y^m is the yield stress of the metal. The ratio between these two groups, $\sigma_{n,s}h/\sigma_Y^m\delta_{n,s}$, defines a normalized interfacial stiffness. Various values of $\sigma_{n,s}/\sigma_Y^m(10^{-2}\text{–}10^1)$, $\delta_{n,s}/h\ (10^{-3}\text{–}10^2)$ will be used in the simulation. We first assume
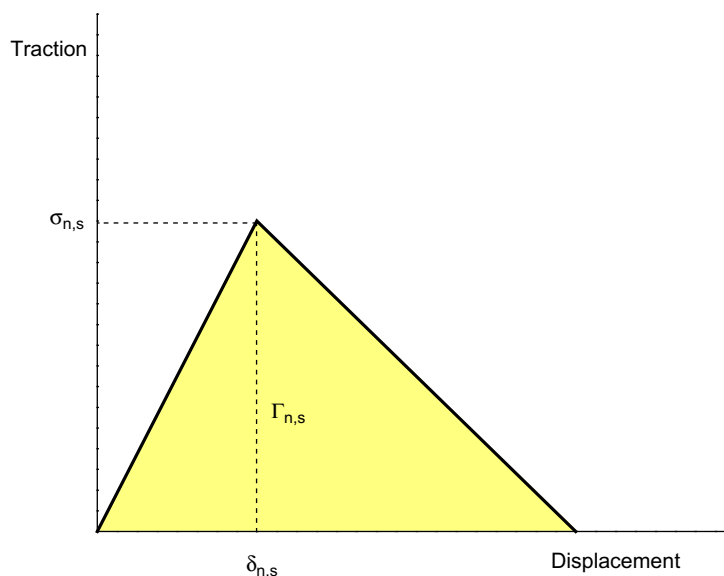

Fig. 3. The traction–separation laws used to model the metal/polymer interface.

that $\sigma_n = \sigma_s$ and $\delta_n = \delta_s$, and then introduce different opening and shearing properties to identify the adhesion parameters governing the necking process. Our simulations show that, once the interface strength $\sigma_{n,s}$ and the corresponding displacements $\delta_{n,s}$ are fixed, the tails of the traction–displacement laws are of secondary importance to the rupture process of the metal films on the polymer substrates. Consequently, we will not discuss our results in terms of Γ_n and Γ_s.

3. Three types of tensile behavior

Depending on the interfacial strengths $\sigma_{n,s}/\sigma_Y^m$ and the corresponding interfacial displacements $\delta_{n,s}/h$, three types of tensile behavior can be identified. Type I behavior occurs when the interface strength is very low or the corresponding interfacial displacement is very large (i.e., in Fig. 4a, $\sigma_{n,s}/\sigma_Y^m = 10^{-2}$ and $\delta_{n,s}/h = 1$). The film forms a single neck near the preexisting notch, and also debonds from the substrate. The interfacial debonding and the film necking proceed simultaneously and facilitate each other. The notch starts thinning at a strain of about 2%, and the film ruptures at a strain of about 4.6%. As expected, a weak interface cannot constrain the strain localization in the metal film.

Type II behavior occurs when the interfacial strength and the corresponding interfacial displacement are of intermediate values (i.e., in Fig. 4b, $\sigma_{n,s}/\sigma_Y^m = 0.5$ and $\delta_{n,s}/h = 0.05$). The film forms *multiple necks*, stretches to a *much larger strain*, and then ruptures near the preexisting notch. The development of the multiple necks is accompanied by debonding at multiple locations where necking occurs. The large rupture strain can be readily understood as follows. Each neck contributes an extra elongation of about one film thickness, h. As a whole, the metal film can stretch to a large strain before final rupture. Further simulations show that, as the interfacial strengths increase and the corresponding interfacial displacements decreases, the spacing between the necks decreases and the rupture strain increases.

Type III behavior occurs when the interfacial strength is high and the corresponding interfacial displacement is small (i.e., in Fig. 4c, $\sigma_{n,s}/\sigma_Y^m = 1$ and $\delta_{n,s}/h = 0.005$), the metal films can deform uniformly to very large strains without rupture. No appreciable debonding occurs at the interface.

Fig. 5 plots a map on a plane spanned by the two dimensionless groups, $\delta_{n,s}/h$ and $\sigma_{n,s}/\sigma_Y^m$. Each data point corresponds to a case of finite element simulation. According to the data points, we estimate the boundaries between neighboring types of tensile behavior. In the region of the type II behavior, the density of the necks in the film gradually increases from the bottom to the top and from the right to the left in the map. Indeed, in some region of the type II behavior, where $\sigma_{n,s}/\sigma_Y^m \geqslant \sim 0.5$ and $\sigma_{n,s}h/\sigma_Y^m\delta_{n,s} \geqslant \sim 5$, the metal film can form multiple necks but deform to very large strain (i.e., more than 60%) without rupture.

Type I $(\varepsilon = 4.6\%, \sigma_{n,s}/\sigma_Y^m = 10^{-2}, \delta_{n,s}/h = 1)$

Type II $(\varepsilon = 40\%, \sigma_{n,s}/\sigma_Y^m = 0.5, \delta_{n,s}/h = 0.05)$

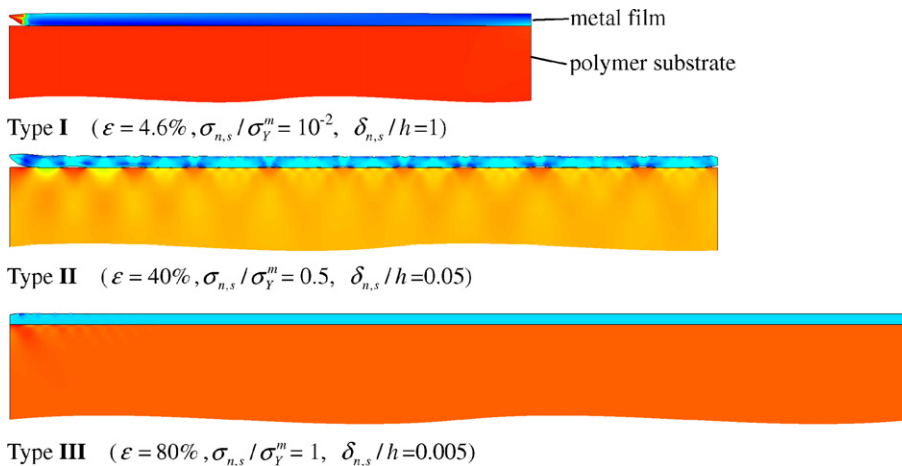Type III $(\varepsilon = 80\%, \sigma_{n,s}/\sigma_Y^m = 1, \delta_{n,s}/h = 0.005)$

Fig. 4. Finite element simulations identify three types of tensile behavior, depending on the interfacial strengths and the corresponding interfacial displacements. The right half of the laminate and only top part of the substrate are shown. Shades represent the Mises stress level. Note the much larger strains in the types II and III behavior.
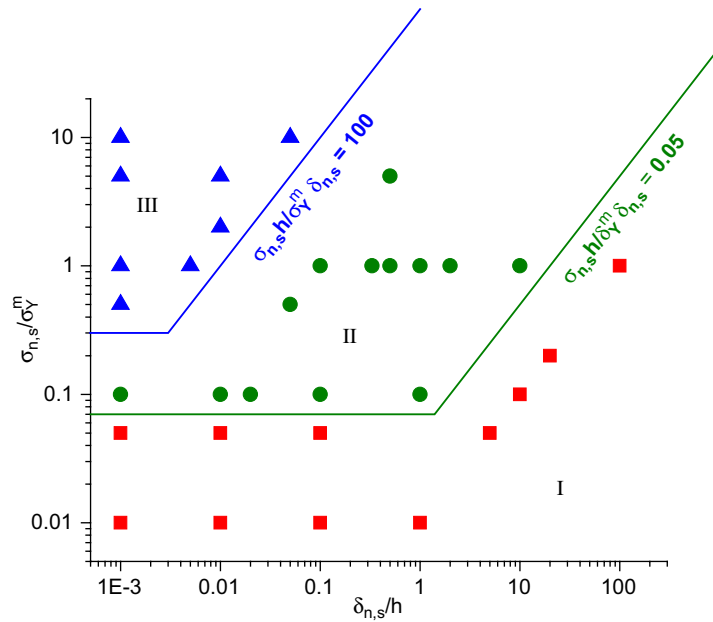
Fig. 5. A map of tensile behavior of thin metal films on polymer substrates, on a plane spanned by interfacial strengths $\sigma_{n,s}/\sigma_Y^m$ and corresponding interfacial displacements $\delta_{n,s}/h$. The three types of tensile behavior are denoted by I, II and III.

Fig. 6 plots the rupture strain as a function of the normalized interfacial stiffness for several levels of the interfacial strength. The rupture strain increases as the normalized interfacial stiffness increases. Such an increase is negligible if the interfacial strength is too low (i.e., $\sigma_{n,s}/\sigma_Y^m = 0.01$), but becomes substantial if the interfacial strength is high (i.e., $\sigma_{n,s}/\sigma_Y^m = 1$).
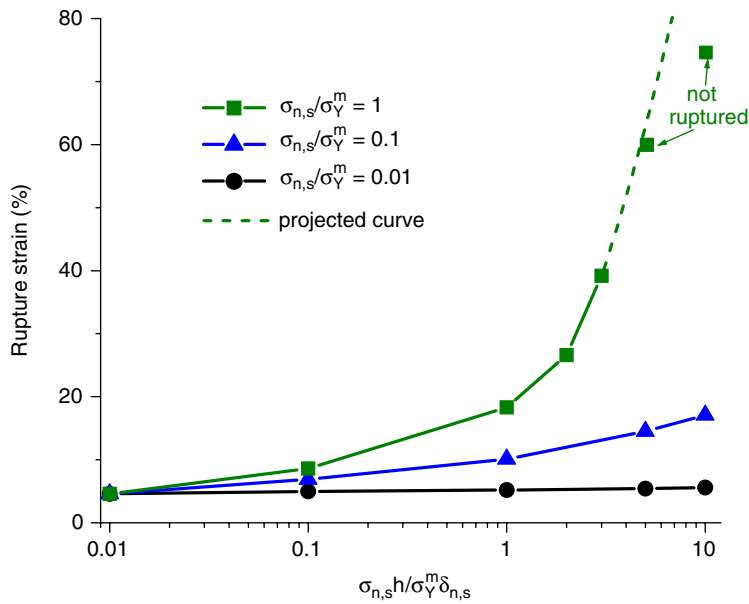

Fig. 6. Rupture strain as a function of normalized interfacial stiffness for various interfacial strengths.

4. Necking in the film is accommodated by interfacial sliding

As discussed in Section 1, if a metal film on a polymer substrate ruptures at a small strain by forming a single neck, the interface should debond over a length many times the film thickness. This prediction, however, is not immediately evident in Fig. 4a. To further elucidate the co-evolution of the interfacial debonding and the film necking, Fig. 7 plots the interfacial sliding/opening displacements of a laminate at various stages during a deformation sequence. The origin of spatial coordinates is set at the center of the film/substrate interface. Let x_1 axis coincide with the metal/polymer interface, pointing to the direction of applied strain.
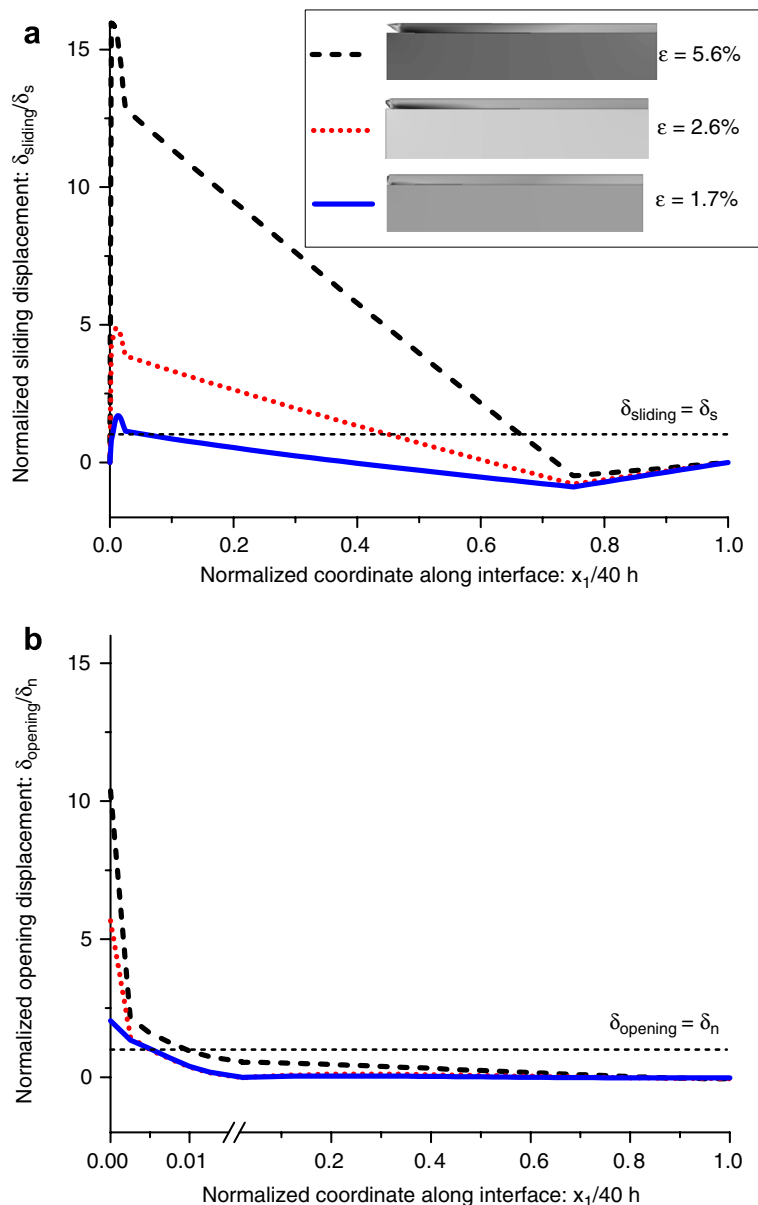

Fig. 7. (a) The sliding displacement δ_{sliding} and (b) the opening displacement δ_{opening} along the interface at various applied strains of 1.7%, 2.6% and 5.6%. The deformed shapes of the laminate at these strains are shown in the legend. The horizontal axis in (b) is rescaled near the necking region to show details. In this simulation, $\sigma_{\text{n,s}}/\sigma_Y^{\text{m}} = 0.01$ and $\delta_{\text{n,s}}/h = 0.1$.

The film starts to debond and neck near the preexisting notch at a strain of 1.7% and ruptures there at a strain of 5.6%. Fig. 7a and b plot the sliding displacement δ_{sliding} and the opening displacement δ_{opening} along the interface, respectively, at various applied strains of 1.7%, 2.6% and 5.6%.

As shown in Fig. 7, large amplitude of sliding and opening displacements (i.e., $\delta_{\text{sliding}} > \delta_s$ and $\delta_{\text{opening}} > \delta_n$) occur at the interface near the preexisting notch at a strain of 1.7%, which initiate the interfacial debonding and the film necking. As the strain increases, the sliding displacement of increasing amplitude spread over the interface, leading to the propagation of interfacial debonding. By contrast, the opening displacement is significant only near the imperfection and is negligible at the rest of the interface.

Fig. 7 shows that the interfacial debonding and the film necking facilitate each other; furthermore, the necking of the film is mainly accommodated by interfacial sliding, rather than interfacial opening. In Fig. 7a, the sliding-induced debonding at the rupture strain of 5.6% is of length $L \approx 26h$. (The negative sliding displacement ahead of the debonding front results from the prescribed displacement at the right side of the laminate.) The simple estimation of Eq. (1) with such a debonding length gives a rupture strain of about 5.8%. The estimate agrees with the FEM result within 5%.

Given the unbalanced contribution from interfacial sliding and opening, it is necessary to compare the effects of the interfacial shear strength and the interfacial tensile strength on the rupture strains. As shown in Fig. 8, compared with an interface with equal interfacial strengths ($\sigma_n/\sigma_Y^m = \sigma_s/\sigma_Y^m = 0.01$–$0.1$), an interface with higher interfacial tensile strength ($\sigma_n/\sigma_Y^m = 1$ and $\sigma_s/\sigma_Y^m = 0.01$–$0.1$) results in a negligible increase in the rupture strains. By contrast, an interface with higher interfacial shear strength ($\sigma_s/\sigma_Y^m = 1$ and $\sigma_n/\sigma_Y^m = 0.01$–$0.1$) leads to rupture strains more than twice of that if the interfacial strengths are equal. Consequently, for a given normalized interfacial stiffness ($\sigma_{n,s}h/\sigma_Y^m\delta_{n,s} = 10$ in Fig. 8), the rupture strain of the metal films on polymer substrates is more sensitive to the interfacial shear strength, rather than the interfacial tensile strength.
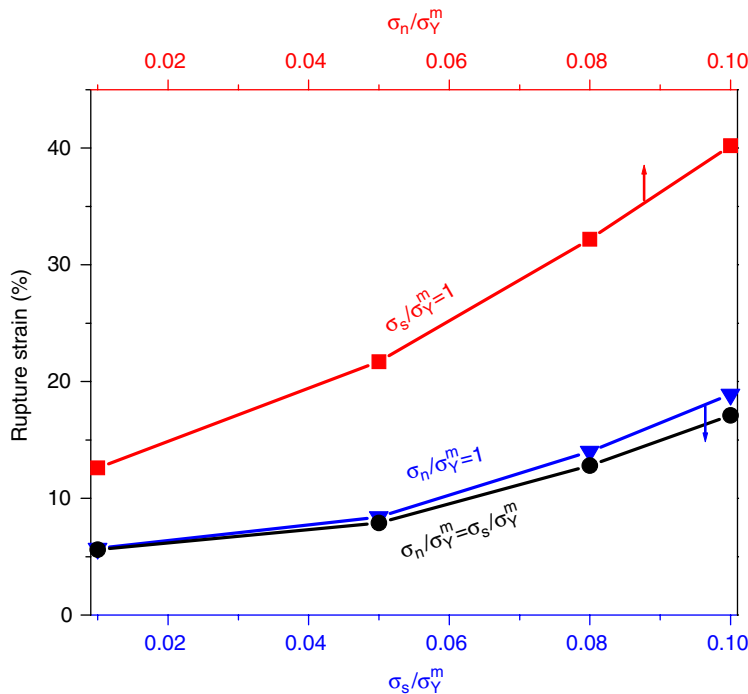

Fig. 8. Rupture strain as a function of interfacial strength for laminates with higher interfacial shear strength (square), higher tensile strength (triangle) and equal shear and tensile strength (circle). The normalized interfacial stiffness is $\sigma_{n,s}h/\sigma_Y^m\delta_{n,s} = 10$.

5. Discussion

The three types of deformation behavior of metal films on polymer substrates identified in this paper parallel our previous results on metal films well-bonded on elastomer substrates (Li et al., 2004; Li and Suo, 2006). In that study, depending on the elastic modulus of the substrate (1–200 MPa), the metal films show the three similar types of tensile behavior. This similarity suggests that the metal/polymer interface is analogous to a set of springs. The substrate constraint to the strain localization in the film acts through these springs, and the rupture strain is governed by the normalized spring constants of $\sigma_{n,s} h / \sigma_Y^m \delta_{n,s}$ and normalized spring strengths of $\sigma_{n,s}/\sigma_Y^m$. If the springs are too compliant or too weak, the film can easily slide along the interface or separate from the substrate, providing space to accommodate the local elongation near the neck, thus leading to a small rupture strain.

The sliding-induced debonding is of particular significance in the metal-on-polymer system. While chemical bonds prevail inorganic–inorganic interface (i.e., Cu/SiO_2), the metal/polymer interface mainly consists of physical bonds, such as van der Waals bonds. Under special treatment during film deposition, chemical bonds can form at the metal/polymer interface. Nonetheless, subject to a tensile strain, the metal and the polymer cannot accommodate the elongation solely by increasing atomic or molecular space. Consequently, certain amount of metal atoms and polymer molecules form new bonds and generate extra interface. These new bonds between metal and polymer are likely to be mostly physical bonds. The strengths of van der Waals bonds are likely not equal, weaker under shear and stronger under tension. The present study suggests that, to achieve larger rupture strain of metal films on polymer substrates, efforts should be placed on increasing the interfacial shear strength and decreasing the corresponding interfacial sliding, not just on improving interfacial adhesion energy.

In the present model, we assume that the laminate deforms under the plane strain conditions; for example, the preexisting notch in the simulations corresponds to an infinitely long trench in the film surface. In real metal films, an imperfection such as a missing grain may initiate nonuniform deformation, which then propagates across the film, leaving a long neck in its wake, as illustrated in Fig. 2. Rupture by this process requires higher applied strain than that of the rupture originated by a long trench in the film. In practice, the metal/polymer laminates may be subject to biaxial tensile strains. Under such loading, an imperfection in the film may develop to a neck in a direction, not necessarily coinciding with one of the loading direction, but related to the biaxial loading ratio, metal/polymer geometry and their mechanical behaviors. Further study of the co-evolution of debonding and necking in a metal/polymer laminate under biaxial strains will be reported elsewhere.

6. Summary

When a metal/polymer laminate is subject to a modest tensile strain, debonding may occur along the interface and the strain localization (i.e., necking) may occur in the film. These two processes – debonding and necking – facilitate each other, leading to the rupture of the film. We simulate the co-evolution of film necking and interfacial debonding, and identify three types of tensile behavior of the laminate. If the interface is very weak or very compliant, the film debonds and ruptures by forming a single neck at a small strain. If the interface is strong and stiff, the metal film deforms uniformly to a very large strain without debonding. If the interface is of intermediate strength and stiffness, the film partially debonds and deforms to a large strain by forming multiple necks. The simulation also shows that the necking of the film is mainly accommodated by interfacial sliding, rather than interfacial opening.

References

Alaca, B.E., Saif, M.T.A., Sehitoglu, H., 2002. On the interface debond at the edge of a thin film on a thick substrate. Acta Mater. 50, 1197–1209.

Chiu, S.L., Leu, J., Ho, P.S., 1994. Fracture of metal–polymer line structures. J. Appl. Phys. 76, 5136–5142.

Crawford, G.P. (Eds.), 2005. Flexible Flat Panel Displays, Wiley, Hoboken, New York.

Gray, D.S., Tien, J., Chen, C.S., 2004. High-conductivity elastomeric electronics. Adv. Mater. 16, 393–397.

Gruber, P., Böhm, J., Wanner, A., Sauter, L., Spolenak, R., Arzt, E., 2003. Size effect on crack formation in Cu/Ta and Ta/Cu/Ta thin film systems. Mater. Res. Soc. Symp. Proc. 821, P2.7.

Huang, H., Spaepen, F., 2000. Tensile testing of free-standing Cu, Ag and Al thin films and Ag/Cu multilayers. Acta Mater. 48, 3261–3269.

Hutchinson, J.W., Suo, Z., 1992. Mixed-mode cracking in layered materials. Adv. Appl. Mech. 29, 63–191.

Kang, Y.-S., 1996. Ph.D. Dissertation, University of Texas at Austin, Austin, TX.

Li, T., Huang, Z.Y., Lacour, S.P., Wagner, S., Suo, Z., 2004. Stretchability of thin metal films on elastomer substrates. Appl. Phys. Lett. 85, 3435–3437.

Li, T., Huang, Z.Y., Xi, Z.C., Lacour, S.P., Wagner, S., Suo, Z., 2005. Delocalizing strain in a thin metal film on a polymer substrate. Mech. Mater. 37, 261–273.

Li, T., Suo, Z., 2006. Deformability of thin metal films on elastomer substrates. Int. J. Solids Struct. 43, 2351–2363.

Macionczyk, F., Bruckner, W., 1999. Tensile testing of AlCu thin films on polyimide foils. J. Appl. Phys. 86, 4922–4929.

Nathan, A., Chalamala, B.R. (Eds.), 2005. Special Issues on Flexible Electronics Technology, Proc. IEEE 93, 1235–1510.

Pashley, D.W., 1960. A study of the deformation and fracture of single-crystal gold films of high strength inside an electron microscope. Proc. R. Soc. Lond. A 255, 218–231.

Suo, Z., Vlassak, J.J., Wagner, S., 2005. Micromechanics of macroelectronics. China Particuology 3, 321–328.

Xiang, Y., Li, T., Suo, Z., Vlassak, J.J., 2005. High ductility of a metal film adherent on a polymer substrate. Appl. Phys. Lett. 87, 161910.

Xiang, Y., Vlassak, J.J., 2005. Bauschinger effect in thin metal films. Scripta Mater. 53, 177–182.